We are IntechOpen, the world's leading publisher of Open Access books Built by scientists, for scientists

6,900
Open access books available

185,000
International authors and editors

200M
Downloads

Our authors are among the

154
Countries delivered to

TOP 1%
most cited scientists

12.2%
Contributors from top 500 universities

WEB OF SCIENCE™

Selection of our books indexed in the Book Citation Index in Web of Science™ Core Collection (BKCI)

Interested in publishing with us?
Contact book.department@intechopen.com

Numbers displayed above are based on latest data collected.
For more information visit www.intechopen.com

Chapter 4

The Preparation and Hydrogen Storage Performances of Nanocrystalline and Amorphous Mg_2Ni-Type Alloys

Yanghuan Zhang, Hongwei Shang, Chen Zhao and Dongliang Zhao

Additional information is available at the end of the chapter

http://dx.doi.org/10.5772/50281

1. Introduction

The earth owning better environment, including fresh air, clean rain and healthy sunshine, is always the best wish of human. However, statistics indicate that air pollution and the greenhouse effect are becoming more and more serious caused by exhaust gas of vehicles, which seriously endanger human health. Petroleum fuels are the chief criminal. Furthermore, petroleum fuels belong to non-renewable resources, which need a long time to recycle and the reserves are limited. Especially in China, along with the development of domestic economy, the heavy demand of cars is taking on unceasing climbing in a straight line. The difficulties we met are more serious. Therefore, under this precondition, the need of seeking a kind of convenient, clean efficient sources of energy is a very pressing task for researchers. China provides broad space for clean energy exploitation, including solar, hydrogen, and wind power. Right now, the researches focus on hydrogen due to some advantages. As is known to everybody, hydrogenous sources of energy is widespread, such as water covers most of the earth surface and a wide range of hydride exists in natural gas, coal, plants on earth, providing an inexhaustible resource for our society.

Hydrogen energy is a kind of high efficient, clean secondary energy. However, hydrogen storage is one of the main obstacles in hydrogen utilization. The traditional way such as high pressure tanks and liquid hydrogen tanks are once regarded as candidates for road tests, but it is proved from practice that these ways have certain fatal flaws in some respects. These methods not only occupy a large space of cars but also put in safe hidden trouble. In addition, both high pressure tanks and liquid hydrogen tanks are facing another problem — the lack of hydrogen refueling stations. The cost of hydrogen refueling which is far beyond than that of gasoline filling station, revealing the reasons why most of the major oil

INTECH
open science | open minds

© 2012 Zhang et al., licensee InTech. This is an open access chapter distributed under the terms of the Creative Commons Attribution License (http://creativecommons.org/licenses/by/3.0), which permits unrestricted use, distribution, and reproduction in any medium, provided the original work is properly cited.

companies have been loathed to set up hydrogen refueling stations. In comparison with the above traditional methods, alloy hydrides with lots of advantages such as high hydrogen storage capacity, good reversibility and low cost have been identified as an ideal fuel for many energy converters in recent years [1]. Electrochemical hydrogen storage is a more convenient method, by which atomic hydrogen is adsorbed in hydrogen storage materials during electrochemical decomposition of an aqueous medium [2]. The only product of the whole reaction is just water. So, it is "totally clean" and extremely useful for application to emerging vehicles based on hydrogen fuel cell technologies.

At present, the new energy resources cars mainly involve Hybrid Electrical Vehicle (HEV) and electric vehicles (EV). Substituting petrol-driven car with HEV and EV has been a primary way for solving the above environmental problems for researchers in this area. Compared with the traditional cars, the usage cost of EV and HEV have been reduced to some extent in recent years. So far, the current new energy vehicles in market, primarily uses Ni/MH batteries, lead-acid batteries, and lithium iron phosphate batteries. Lead-acid batteries are usually used in the start-up process of vehicles. The performance of Lithium iron phosphate batteries is more outstanding than Ni/MH batteries. The Chevy Volt, relying on lithium ion batteries, is able to travel 65 km on a single charge. However, it is reported that lithium batteries may be caught fire or exploded after certain overheating, which is a major drawback for its application and development. Among all the batteries, Ni/MH batteries make maximum potential due to it being the most technically matured. And it gets the most extensive of application. Predictably, Ni/MH batteries will still occupy a market share in the first place in the future development of the new energy vehicles. Therefore, in order to occupy the future market, some famous auto manufacture enterprises already have brought some hybrid or electric cars to market. Renault and Nissan are developing electric cars and forecast that plug-in hybrids will become the mainstream products. In the mean time, Toyota plans to start global trials of 500 plug-in hybrids. It is well known that China is always investing heavily in cleaner cars. In the "863" High-tech Plan, "973" Plan and the National Natural Science Foundation, hydrogen storage material is limited as one of the key research areas. China carmakers even have a chance to leapfrog an entire generation of automotive technology and narrowing the gap with developing countries by actively participating in the new energy vehicle development, according to some industry observers. This show the importance and necessity of giving priority to the development of new energy vehicles. Chang'an Jie Xun is the domestic first hybrid cars. Chery Automobile's new A5 also have been available to Chinese consumers whose price is less than 80000 RMB. In addition to the above-mentioned new energy vehicles, Faw-Besturn and Buick Lacrosse are also Eco-friendly cars which using Ni/MH battery as energy supplying device. Yet, barriers against running cars with hydrogen is still quite tough. As an on-board secondary batteries, Ni/MH battery must have higher capacity and good gaseous and electrochemical hydriding and dehydriding kinetics for enhancing the electric power continue voyage.

The negative electrode is a crucial component for hydrogen storage alloy, which is the main bottleneck of Ni/MH batteries for further application. At present, all the Ni/MH batteries

sold in the market adopt $LaNi_5$ hydrogen storage alloy as negative electrode, which was obtained by pure chance in 1969. As a typical commercial alloy, the rare earth based AB_5-type alloy has good cycling stability. Prius is regarded as the iconic founder of Ni/MH rechargeable battery which uses $LaNi_5$ hydrogen storage alloys. For the redesigned Prius, Toyota will stick with the current generation's nickel-metal hydride batteries. However, the discharge capacity of the currently advanced AB_5-type materials has reached 320−340mAh/g at 0.2−0.3C rate at room temperature. It seems to be difficult to further improve the capacity of the AB_5-type alloys since the theoretical capacity of $LaNi_5$ is about 372 mA·h/g [3]. Therefore, the investigations of the new type electrode alloys with higher capacity and good gaseous and electrochemical hydriding and dehydriding kinetics are extremely important to exalt the competition ability of the Ni/MH battery in the rechargeable battery field.

Recently, many researchers have been focused on solving the above problems. And several new and good hydrogen storage alloys were reported., among which the most promising candidates are the Mg and Mg-based metallic hydrides in view of their major advantages such as low specific weight, low cost and high hydrogen capacity, e.g. 7.6 wt.% for MgH_2, 3.6 wt.% for Mg_2NiH_4, 4.5 wt.% for Mg_2CoH_5 and 5.4 wt.% for Mg_2FeH_6 [4,5]. However, the commercial application to hydrogen suppliers has been limited mainly due to their sluggish hydriding/dehydriding kinetics as well as high thermodynamic stability of their corresponding hydride. Therefore, the investigation in this area has been focused on finding the ways to substantially ameliorate the hydriding/dehydriding kinetics of Mg and Mg-based alloys. Various attempts, particularly mechanical alloying (MA) [6] and melt spinning [7], have been conducted to ameliorate the kinetic property of Mg-based metallic hydrides. And the worldwide researchers have carried out a lot of investigations and have obtained some extremely important results. It was documented that Mg and Mg-based alloys with a nanocrystalline/amorphous structure exhibit higher H-absorption capacity and faster kinetics of hydriding/dehydriding than crystalline Mg_2Ni, which is ascribed to the enhanced hydrogen diffusivity and solubility in amorphous and nanocrystalline microstructures [8,9]. It was reported that the addition of third element greatly facilitates the glass forming of the Mg–Ni-based alloys[10,11] and that the partial substitution of M (M=Co, Cu) for Ni in Mg_2Ni compound decreases the stability of the hydride and makes the desorption reaction easier [12].

2. Preparation of alloys

It has come to light that high energy ball-milling (HEBM) has been regarded as a very effective method for the preparation of nanocrystalline and amorphous Mg and Mg-based alloys. Particularly, it is suitable to solubilize particular elements into MgH_2 or Mg_2NiH_4 above the thermodynamic equilibrium limit, which is helpful to destabilize MgH_2 or Mg_2NiH_4 [13]. However, the milled Mg and Mg-based alloys exhibit very poor hydrogen absorbing and desorbing stability in the light of the evanishment of the metastable structures formed by ball milling during the multiple hydrogen absorbing and desorbing cycles [14] . Furthermore, the HEBM process has some insurmountable disadvantages such as the necessity of long times to produce an amorphous alloy, difficulty for mass-

production, and contamination from the chamber and balls used in ball-milling. Alternatively, the melt-spinning technique is the most useful method to obtain an amorphous and/or nanocrystalline phase in the absence of disadvantages inherent to the HEBM process and is more suitable for mass-production of amorphous alloys. Now, vacuum rapidly quenching technologies are used in the preparation of various metals and alloys, and the nano-crystalline and amorphous structures are obtained. The principle of the melt spinning technology is that the liquid metal and alloy can be solidified at great degree of super cooling by means of vacuum rapidly quenching. It was reported that nanocrystalline alloys produced by melt-spinning could have excellent hydriding characteristics even at room temperature, similar to the alloys produced by the HEBM process[15,16].

In order to improve the hydriding and dehydriding kinetics of the Mg_2Ni-type alloy, Ni in the alloy was partially substituted by element M (M=La, Co, Cu,). We have investigated systematically the effect of M (M=La, Co, Cu,) partial substitution for Ni on the microstructure characteristics, gaseous and electrochemical hydriding and dehydriding kinetics properties. The compositions of the alloys were $Mg_{20-x}La_xNi_{10}$ (x=0-6) and $Mg_{20}Ni_{10-x}M_x$ (M=Co, Cu; x=0, 1, 2, 3, 4). The experimental alloys were prepared by using a vacuum induction furnace in a helium atmosphere at a pressure of 0.04 MPa in order to prevent the volatilization of element Mg during melting. A part of the as-cast alloys was re-melted and spun by melt spinning with a rotating copper roller cooled by water, and the ribbons with width of 5 mm and thickness of 20 to 30 μm were obtained. The spinning rate, a very important parameter, was approximately expressed by the linear velocity of the copper roller because it is too difficult to measure a real quenching rate i.e. cooling rate of the sample during quenching. The spinning rate used in the experiment was 15, 20, 25 and 30 m/s, respectively.

3. Detection method

The phase structures of the as-cast and spun alloys were determined by XRD (D/max/2400). The morphologies of the as-cast alloys were examined by SEM (Philips QUANTA 400). The thin film samples of the as-spun alloys were prepared by ion etching for observing the morphology with HRTEM (JEM-2100F), and for determining the crystalline state of the samples with electron diffraction (ED). The thermal stability of the nanocrystalline and amorphous alloys was determined by Differential Scanning Calorimetry (DSC) instrument (STA449C).

The gaseous hydriding and dehydriding kinetics of the alloys were measured by an automatically controlled Sieverts apparatus. For comparing the hydriding and dehydriding kinetics performance of the alloys, which substituting Ni with Cu, Co, or Mg with La, the alloys were tested in the same temperature and pressure conditions. In our experiments, the hydriding process was carried out under 1.5 MPa hydrogen pressure (which is the initial pressure of hydriding process) at 200 °C, and the dehydriding process was carried out in vacuum (1×10^{-4} MPa) also at 200 °C.

The electrochemical performances of the as-cast and spun alloys were tested by an automatic galvanostatic system. The electrochemical impedance spectrums (EIS), Tafel polarization curves and hydrogen diffusion coefficient (D) were obtained by an electrochemical workstation (PARSTAT 2273). The alloys were pulverized and then mixed with carbonyl nickel powder in a weight ratio of 1:4. The mixture was cold pressed at a pressure of 35 MPa into round electrode pellets of 10 mm in diameter. Electrochemical measurements were performed at 30 ˚C by using a tri-electrode open cell, consisting of a working electrode (the metal hydride electrode), a sintered $Ni(OH)_2/NiOOH$ counter electrode and a Hg/HgO reference electrode, which were immersed in a 6 M KOH electrolyte. The voltage between the negative electrode and the reference electrode was defined as the discharge voltage. In every cycle, the alloy electrode was firstly charged with a constant current density, and following the rest of 15 min, and then discharged at the same current density to cut-off voltage of –0.5 V.

For the potentiostatic discharge, the test electrodes in the fully charged state were discharged at 500 mV potential steps for 3500s on electrochemical workstation (PARSTAT 2273), using the CorrWare electrochemistry corrosion software.

4. Results and discussion

Element substitution is one of the radical approaches of improving the performance of materials. And based on our former works, we can conclude that the melt spinning can improve the gaseous and electrochemical hydriding and dehydriding kinetics. Therefore, in our studies, we tried to obtain new type hydrogen storage alloys, which have predominant gaseous and electrochemical hydriding and dehydriding kinetics while maintaining good overall performance by the above two methods. It is well known that Mg_2Ni belongs to A_2B-type hydrogen storage alloys, in which Mg represents the A side elements while Ni represents the B side elements. They act differently from each other. Generally, researchers substitute A side element with La, Ce, Pr, Nd, Sm and substitute B side element with Co, Cu, Mn, Al, Zr for improving the gaseous and electrochemical hydriding and dehydriding kinetics. For the sake of simplicity, I will only introduce partial research results of our research team to illustrate the effect of element substitution, such as substituting La for Mg and Co, Cu for Ni, together with the effect of the melt spinning, such as the spun rate being 5, 10, 15, 20, 25m/s, respectively.

4.1. The effect of substituting Mg with La on microstructure characteristics as well as the gaseous and electrochemical hydriding and dehydriding kinetics

4.1.1. Microstructure characteristics

Fig. 1 shows the ribbons which obtained by substituting Mg with La (x=2) and melting spinning as the spun rate being 20m/s. It is about 5 mm wide and 20 to 30 μm thick by measurement.

The XRD patterns of the as-cast and spun $Mg_{20-x}La_xNi_{10}$ (x=0-6) alloys are shown in Fig. 2. It is evident that no amorphous phase is detected in the as-spun La_0 alloy, but all the as-spun

alloys substituted by La display an obvious amorphous structure, suggesting that the substitution of La for Mg facilitates the glass forming of the Mg_2Ni alloys.

Figure 1. Actual picture of the as-spun (20 m/s) La_2 alloy

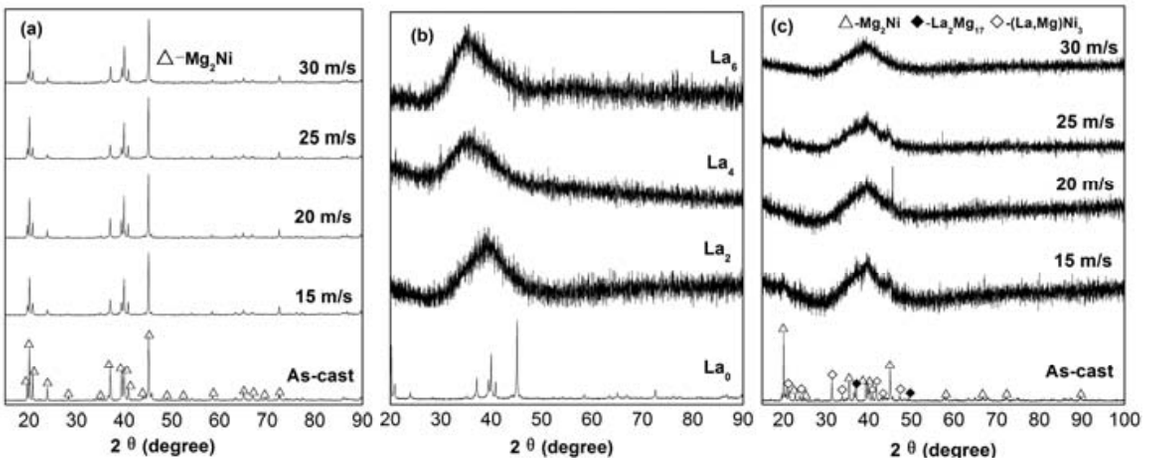

Figure 2. XRD patterns of the as-cast and spun (30 m/s) alloys: (a) La_0 alloy, (b) As-cast and quenched alloys, (c) La_2 alloy

The HRTEM images of the as-spun (30 m/s) alloys are illustrated in Fig. 3. It can be seen that the as-spun La_0 alloy displays a complete nanocrystalline structure, and its electron diffraction (ED) pattern appears sharp multi-haloes corresponding to a crystal structure. The morphologies of the as-spun La_2 and La_4 alloys exhibit a feature of the nanocrystalline embedded in the amorphous matrix. The morphology of the as-spun La_6 alloy shows a nearly complete amorphous character, and its electron diffraction pattern consists of only broad and dull halo, displaying an amorphous structure. It is noteworthy that the amount of the nanocrystalline in the as-spun alloys clearly decreases with increasing La content, meaning that the substitution of La for Mg increases the glass forming ability of the M_2Ni-type alloy, which agrees very well with the results of the XRD observation. Two elucidations can be regarded as the reasons for the above result. On the one hand, the addition of third element to Mg-Ni or Mg-Cu alloys facilitates the glass-formation [17]. On the other hand, the glass forming ability of an alloy is closely associated with the difference of the atomic

radii in the alloy. The larger difference between the atom radii suggests the higher glass forming ability [18].

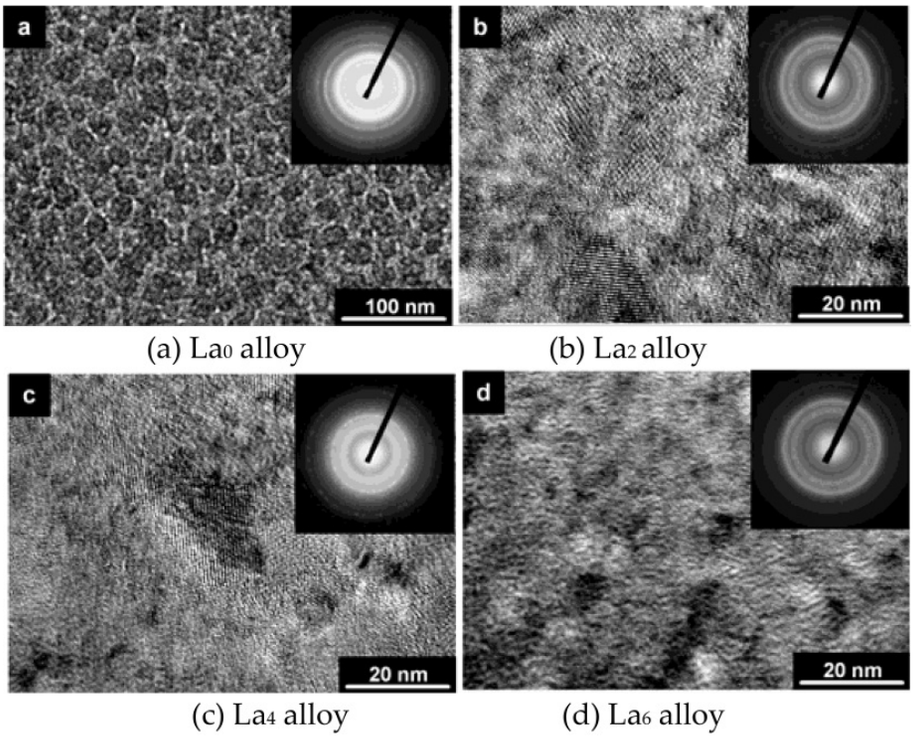

Figure 3. HRTEM micrographs and ED patterns of the as-spun (30 m/s) alloys

4.1.2. Thermal stability and crystallization

In order to examine the thermal stability and the crystallization of the as-quenched amorphous and nanocrystalline/amorphous alloys, DSC analysis was conducted. The resulting profiles shown in Fig. 4 reveals that during heating the alloys crystallized completely, and the crystallization process of La_2 alloy consisted of several steps. The first crystallization reaction at about 210 °C is connected with a sharp exothermic DSC peak, followed by a smaller and wider peak (312 °C) corresponding to a second crystallization reaction. At higher temperatures (at about 396 °C) a third exothermic effect can be detected. It was proved that the first sharper peak corresponds to the crystallization (ordering) of the amorphous into nanocrystalline Mg_2Ni [19]. Based on the results in Fig.2 (c), it was speculated that the second and the third exothermic peaks correspond to the crystallization of the amorphous into nanocrystalline (La, Mg)Ni_3 and La_2Mg_{17}, respectively. It was also seen that the crystallization temperatures of the alloys slightly rose with the increasing quenching rate, which was probably relevant to the influence of the quenching rate on the amorphized degree of the alloy.

4.1.3. Gaseous and electrochemical hydriding and dehydriding kinetics

The hydrogen absorption curves of as-cast and spun La_0 and La_2 alloys are presented in Fig. 5. Upon the first contact with hydrogen at 200 °C and 1.5 MPa, the activated alloys rapidly

absorb copious amounts of hydrogen, and the initial hydriding rate increases with the rising of the spinning rate. The hydrogen absorption capacity in 10 min is increased from 1.21 to 3.10 wt% for the La_0 alloys, and from 1.26 to 2.60 wt% for the La_2 alloy by growing spinning rate from 0 to 30 m/s, indicating that the hydrogen absorption capacity and kinetics of all the as-spun alloys studied are superior to those of conventional polycrystalline materials with similar composition. The improved hydrogen absorption characteristics are attributed to the amorphous and nanocrystalline microstructures created by melt spinning in the light of those structure displaying high hydrogen diffusivity and solubility. In order to reveal the mechanism of the melt spinning improving hydrogen absorption kinetics of the alloy, it is evidently necessary to investigate the influences of the melt spinning on the hydrogen diffusion ability in the alloy. The hydrogen diffusion coefficients in the as-cast and spun alloys were measured using the potential step technique.

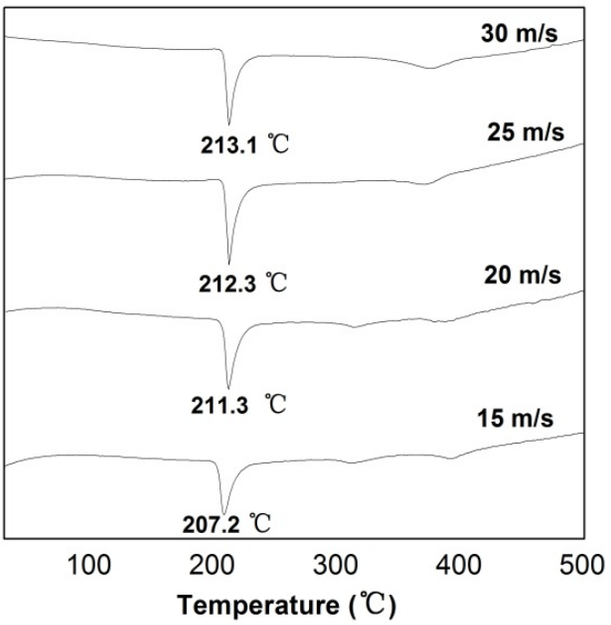

Figure 4. DSC profiles of La_2 alloy quenched at different quenching rates

Fig. 6 shows the semilogarithmic curves of anodic current versus working duration of the as-cast and spun alloys. The diffusion coefficient D of the hydrogen atoms in the bulk of the alloy can be calculated by following formulae [20]:

$$\log i = \log\left(\pm\frac{6FD}{da^2}\left(C_0 - C_s\right)\right) - \frac{\pi^2}{2.303}\frac{D}{a^2}t \tag{1}$$

$$D = -\frac{2.303a^2}{\pi^2}\frac{d\log i}{dt} \tag{2}$$

The D values are also illustrated in Fig. 6, indicating that the melt spinning has a visible effect on hydrogen diffusion in the alloy. As the spinning rate grows from 0 to 30 m/s, the hydrogen diffusion coefficient D always increases from 1.350×10^{-11} to 2.367×10^{-11} cm^2/s for

the La_0 alloy, and from 8.122×10^{-12} to 1.7987×10^{-11} cm^2/s for the La_2 alloy. The above results indicate that a higher spinning rate is always beneficial for enhancing the diffusion ability of hydrogen atoms in the alloys, for which the refined grain and the increased internal stress by melt spinning are mainly responsible due to diffusion coefficient being directly proportional to the internal strain [21].

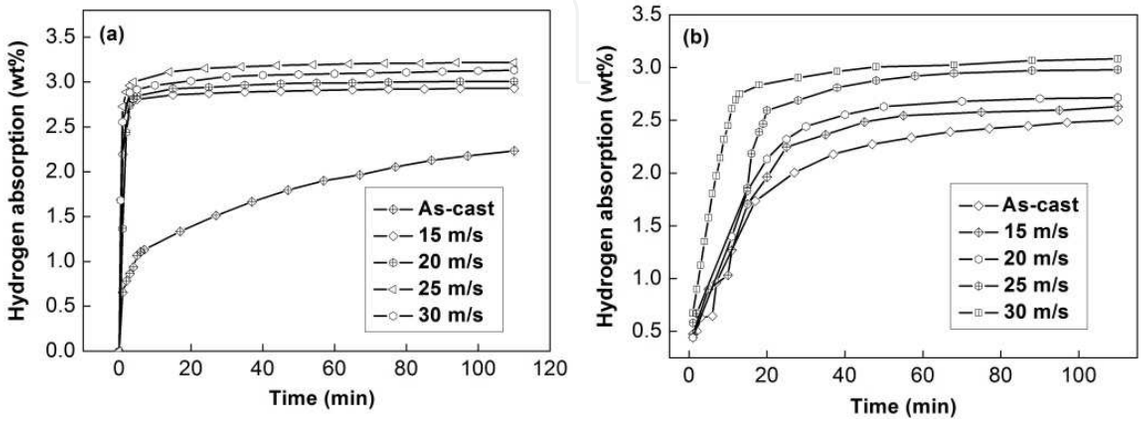

Figure 5. Hydrogen absorption curves of the as-cast and spun alloys: (a) La_0 alloy, (b) La_2 alloy

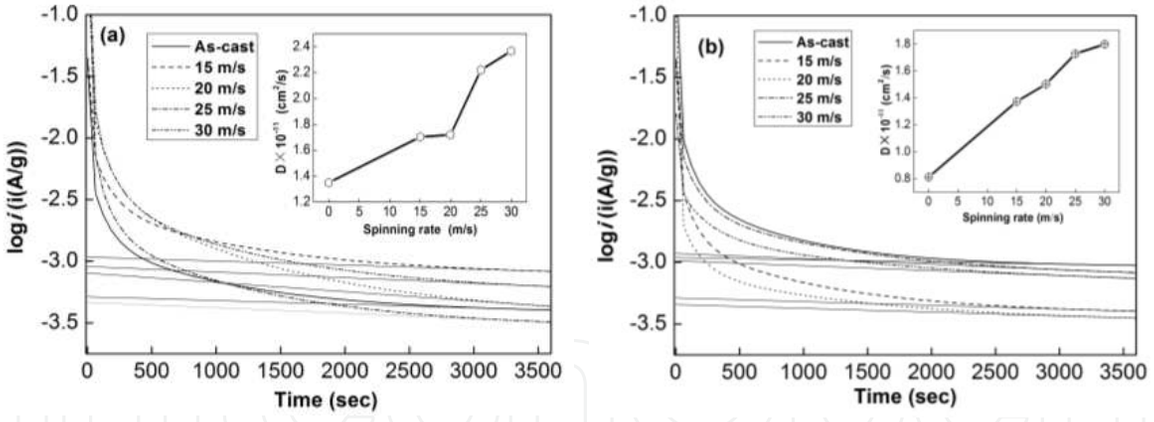

Figure 6. Semilogarithmic curves of anodic current vs. time responses of the as-cast and spun alloy electrodes: (a) La_0 alloy, (b) La_2 alloy

The dehydriding process was carried out in vacuum at 200 °C. The results are shown in Fig. 7. The figures indicate that the hydrogen desorption capacities and kinetics of the alloys are significantly improved by rapid quenching. It can be seen from Fig. 7 that rapid quenching greatly enhanced the hydrogen desorption capacities and improved the dehydrogenation kinetics of the alloys. When the quenching rate rose from 0 to 30 m/s, the hydrogen desorption capacity of the La_0 alloy in 10 min increased from 0.23 to 0.99 wt.%, and from 1.48 to 2.46 wt.% for La_2 alloy, for which the formed nanocrystalline and nanocrystalline/amorphous structures by rapid quenching are mainly responsible.

4.2. The effect of substituting Ni with Co on microstructure characteristics and gaseous as well as electrochemical hydriding and dehydriding kinetics

4.2.1. Microstructure characteristics

The XRD patterns of the as-spun alloys are shown in Fig. 8. It is indicated that the substitution of Co for Ni leads to the formation of secondary phase $MgCo_2$ instead of changing the major phase Mg_2Ni in the alloy. It is evidently visible that the amount of $MgCo_2$ phase grows with the increase in Co content. Fig. 8 displays that no amorphous phase is detectable in the as-spun Co_0 alloy, but the as-spun Co_4 alloy obviously shows the presence of an amorphous phase. Thus, it can be concluded that the substitution of Co for Ni intensifies the glass forming ability of the Mg_2Ni-type alloy. As a third element, Co added to Mg-Ni alloys significantly facilitating the glass formation [17]. Furthermore, the atomic radius of Co is larger than that of Ni, according to the theory of H.S. Chen [18], the glass forming ability of the alloy is enhanced. Table 1 lists the lattice parameters, cell volume as well as the full width at half maximum (FWHM) values of the main diffraction peaks of the as-spun (15 m/s and 30 m/s) alloys, which are calculated by the software of Jade 6.0. It can be derived from Table 1 that the FWHM values of the main diffraction peaks of alloys significantly increase with the increase of the Co content. The substitution of Co for Ni leads to the enlargement of the lattice parameters and the cell volume of alloys. It is also clear in Table 1 that the melt spinning yields the broadened diffusion peaks, indicating the refinement of the average grain size and stored stress in the grains.

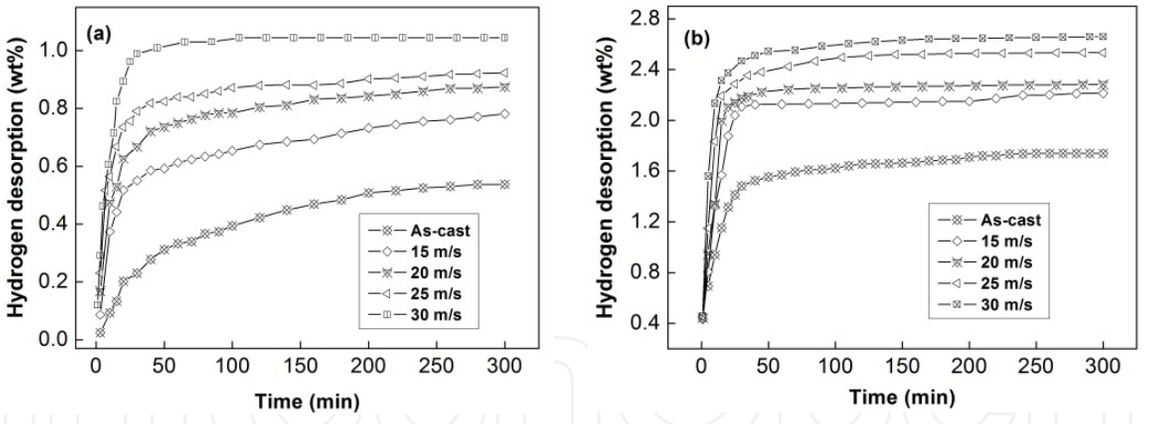

Figure 7. Hydrogen desorption curves of the as-cast and quenched alloys: (a) La_0, (b) La_2

The TEM micrographs of the as-spun (30 m/s) Co_0, Co_1, Co_3 and Co_4 alloys are presented in Fig. 9. It is quite visible that the as-spun Co_0 and Co_1 alloys display a nanocrystalline structure with the grain size of about 20 nm along with the exhibition of their electron diffraction (ED) patterns as sharp multi-haloes. The morphology of the as-spun Co_3 alloy presents a nanocrystalline feature, and a small amount of amorphous phases can be found at its grain boundaries. The Co_4 alloy also exhibits a feature of the nanocrystalline with a grain size of about 20 nm embedded in the amorphous matrix. However, its (Co_4 alloy) electron diffraction pattern consists of broad and dull halo, confirming the presence of an amorphous structure. This result is quite in conformity with the XRD observation shown in Fig. 8.

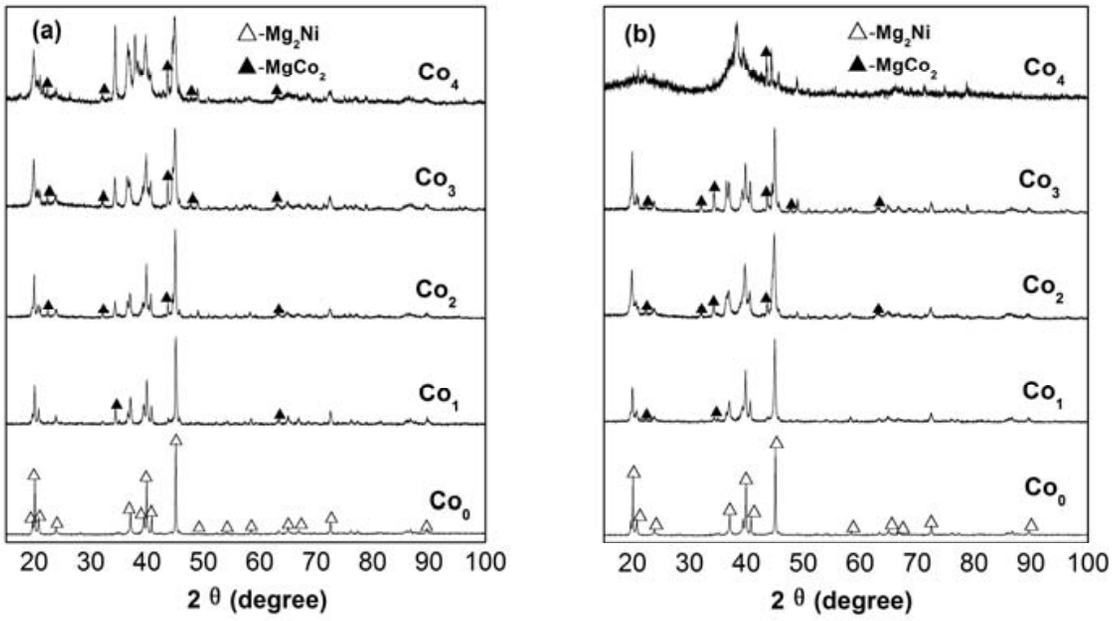

Figure 8. XRD patterns of as-spun alloys with different spinning rates: (a) 15 m/s, (b) 30 m/s

Alloys	FWHM values				Lattice parameters and cell Volume					
	2θ(20.02°)		2θ(45.14°)		a (nm)		c (Å)		V (Å^3)	
	15 m/s	30 m/s	15 m/s	30 m/s	15 m/s	30 m/s	15 m/s	30 m/s	15 m/s	30 m/s
Co_0	0.125	0.133	0.171	0.182	0.5210	0.5211	1.3251	1.3287	0.3115	0.3134
Co_1	0.185	0.206	0.191	0.225	0.5213	0.5219	1.3256	1.3323	0.3120	0.3142
Co_2	0.210	0.246	0.265	0.290	0.5217	0.5285	1.3305	1.3336	0.3136	0.3226
Co_3	0.336	0.536	0.357	0.329	0.5224	0.5287	1.3312	1.3412	0.3146	0.3246
Co_4	0.583	—	0.529	—	0.5225	—	1.3318	—	0.3148	—

Table 1. The lattice parameters, cell volume and the FWHM values of the major diffraction peaks of the alloys

4.2.2. Thermal stability and crystallization

In order to examine the thermal stability and crystallization of the as-spun amorphous and nanocrystalline alloys, DSC analysis has been conducted. The resulting profiles of the as-spun (30 m/s) alloys depicted in Fig. 10 reveal that the crystallization of the as-spun alloys completes during the heating process, furthermore, the crystallization process consists of two steps. The first crystallization reaction is associated with a sharp exothermic DSC peak followed by a smaller and wider peak corresponding to the second crystallization reaction. It is also testified that the first sharper peak corresponds to the crystallization (ordering) of the amorphous into nanocrystalline Mg_2Ni [19]. The crystallization temperature of the

amorphous phase in the as-spun alloys first increases and then decreases with the increasing of Co content.

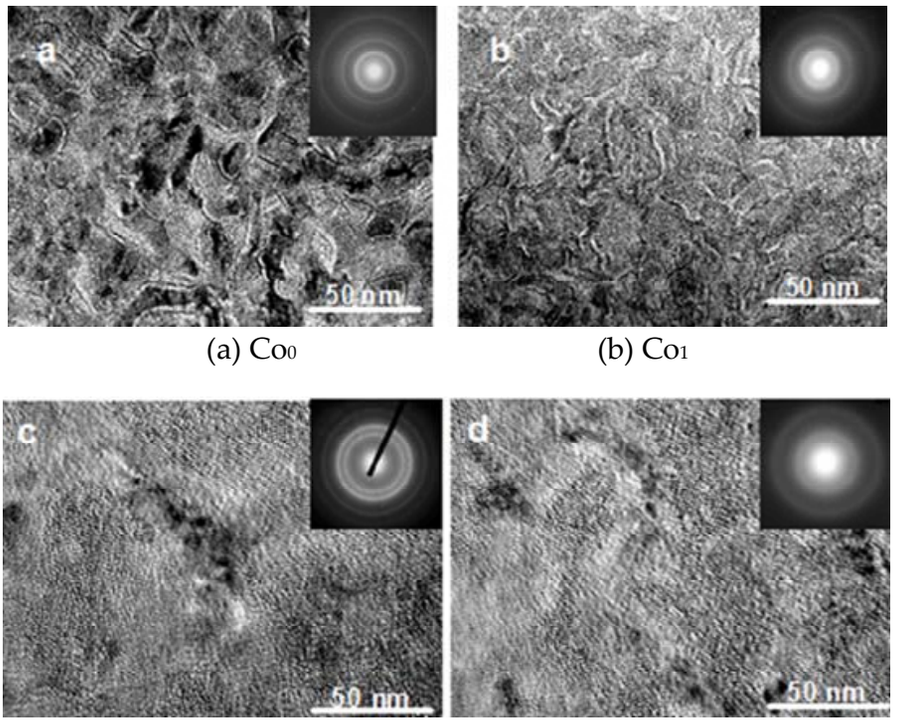

(a) Co_0 (b) Co_1

(c) Co_3 (d) Co_4

Figure 9. TEM images and electron diffraction patterns of as-spun (30 m/s) alloys

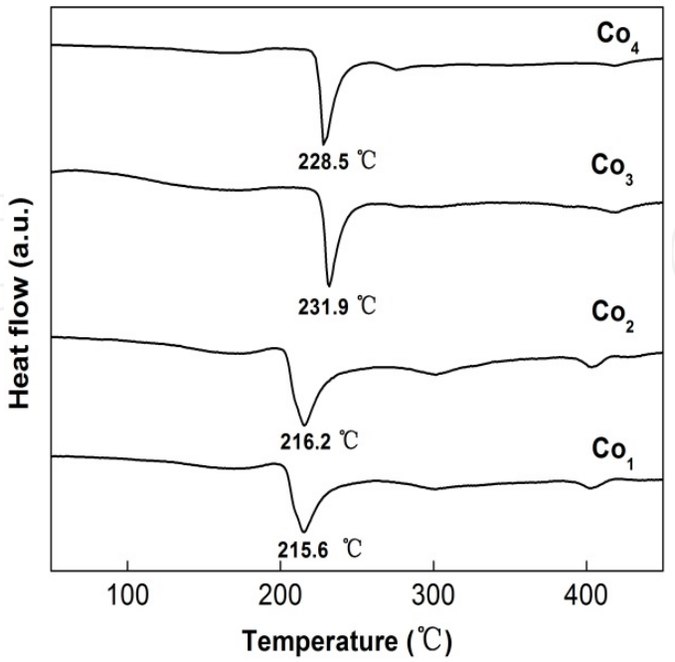

Figure 10. DSC profiles of as-spun (30 m/s) alloys

4.2.3. Gaseous and electrochemical hydriding and dehydriding kinetics

The hydrogen absorption kinetic curves of the as-spun alloys are plotted in Fig. 11. It is visible that all the as-spun alloys demonstrate rapid hydrogen absorption rates and nearly reach their saturation capacities in 10 min. The high hydrogen absorption capacities and fast hydrogen absorption rates of the Co_2 and Co_3 alloys (Fig. 11) may be associated with the increased cell volume resulting from the Co substitution. The hydrogen absorption capacity of the $MgCo_2$ phase is very low, which has resulted in the Co_4 alloy displaying a low hydrogen absorption capacity. The enhancement in the hydrogenation characteristics can be associated with the enhanced hydrogen diffusivity in the amorphous and nanocrystalline microstructures because the amorphous phase around the nanocrystalline leads to an easier access of hydrogen to the nano-sized grains, avoiding the long-range diffusion of hydrogen through an already formed hydride, which is often regarded as the slowest stage of absorption. According to the results reported by Orimo and Fujii [22], the distribution of the maximum hydrogen concentrations in three nanometer-scale regions, i.e. grain region, grain boundary region as well as amorphous region, have been experimentally determined to be 0.3% H in the grain region of Mg_2Ni, 4.0% H at the grain boundary and 2.2% H in the amorphous region. This indicates that the hydrides mainly exist in the grain-boundary region and the amorphous phase region.

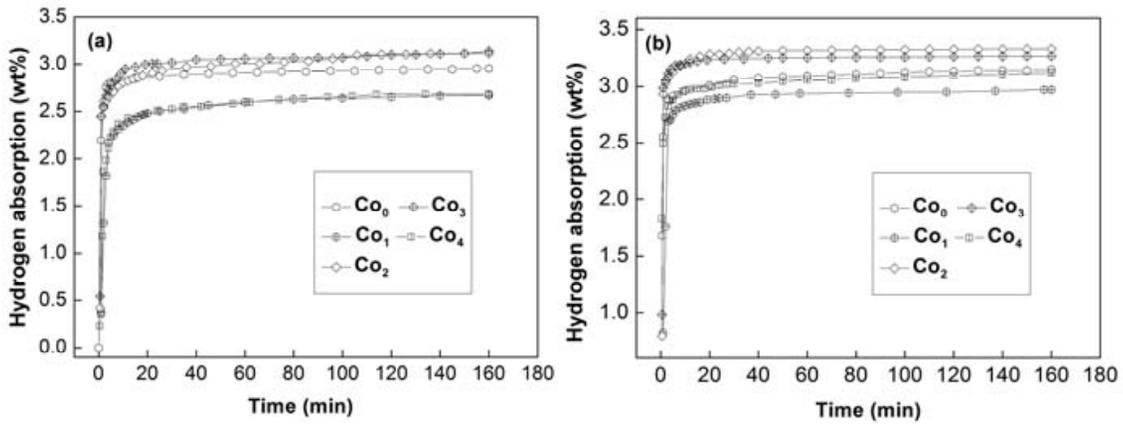

Figure 11. Hydrogen absorption kinetic curves of as-spun alloys: (a) 15 m/s, (b) 30 m/s

The hydrogen absorption kinetic curves of the as-cast and spun Co_1 and Co_4 alloys are plotted in Fig. 12. The results indicate that the hydrogen absorption property of the alloys is significantly enhanced by melt spinning. As the spinning rate grows from 0 to 30 m/s, the hydrogen absorption capacity in 10 min rises from 2.35% to 2.88% for Co_1 alloy, and from 1.91% to 2.96% for Co_4 alloy. These observations indicate that the hydrogenation kinetics and storage capacity of the as-spun nano-crystalline and amorphous Mg_2Ni-type alloys under investigation are superior to those of the conventional polycrystalline materials with similar compositions.

Fig. 13 depicts the hydrogen desorption kinetic curves of the as-spun alloys with spinning rates of 15 m/s and 30 m/s. It is quite visible that the Co substitution significantly

ameliorates the hydrogen desorption capacity and kinetics of the as-spun alloys. As Co content (x) increases from 0 to 4, the hydrogen desorption capacity of the as-spun (15 m/s) alloy in 20 min rises from 0.51% to 1.72%, and from 0.89% to 2.15% for the as-spun (30 m/s) alloy. It is interesting to notice that the hydrogen absorption capacity (Fig. 11) of the as-spun Co_0 alloy is similar to that of the Co_4 alloy, but its hydrogen desorption capability is much lower than that of the Co_4 alloy. Therefore, it can be deduced that the substitution of Co for Ni improves the dehydriding performance of the Mg_2Ni-type alloy. The enhanced hydrogenation characteristics may be ascribed to two reasons. First, the Co substitution significantly intensifies the glass forming ability of Mg_2Ni-type alloy and the amorphous Co for Ni in Mg_2Ni compound lowers the stability of hydride and also Mg_2Ni exhibits an excellent hydrogen desorption capability [23]. Besides, the substitution of facilitates the desorption reaction [12,24].

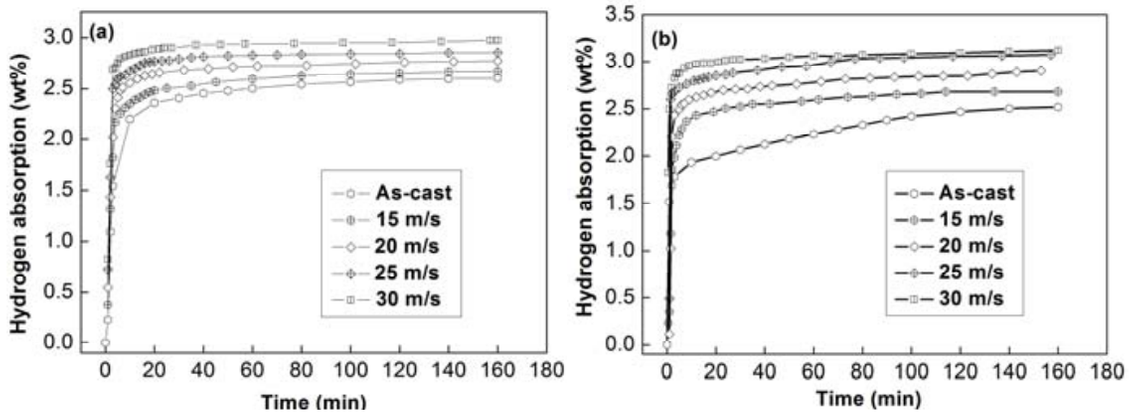

Figure 12. Hydrogen absorption curves of as-cast and spun alloys: (a) Co_1 alloy, (b) Co_4 alloy

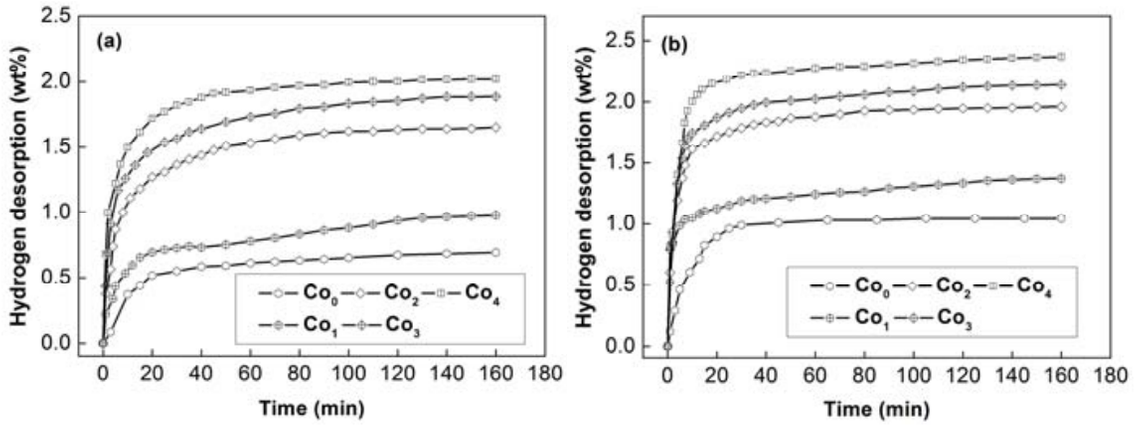

Figure 13. Hydrogen desorption curves of as-spun alloys with different spinning rates: (a) 15 m/s, (b) 30 m/s

Fig. 14 shows the hydrogen desorption kinetic curves of the Co_1 and Co_4 alloys with different spinning rates. The results clearly demonstrate that the dehydriding capability of the alloys increases with the increase of the spinning rate. As the spinning rate grows from 0 to 30 m/s, the hydrogen desorption capacity of the Co_1 alloy in 20 min increases from 0.39%

to 1.13%, and from 1.39% to 2.15% for the Co_4 alloy. In addition, it is clear that the as-cast and spun Co_1 alloy possesses inferior hydrogen desorption capacity and poorer dehydrogenation kinetics comparing to that of the Co_4 alloy. This behavior may be ascribed to the high stability of the crystal Mg-based hydride due to the fact that the melt spinning is unable to change the crystal state of the Co_1 alloy. Hence, the as-spun Co_4 alloy reveals high hydrogen desorption capacity and very fast dehydriding rate. It can be deduced from the aforementioned results that the substitution of Co for Ni significantly ameliorates the hydrogen absorption and desorption capacities and kinetics of the M_2Ni-type alloy. A similar result has already been reported by Khrussanova et al. [25]. The magnesium composites containing 10% and 15% (mass fraction) $Mg_{20}Ni_{10-x}Co_x$ (x=1 and 3) have been prepared by mechanical alloying and it has been found that an intermetallic addition exerts an evident catalytic effect on the hydriding of magnesium. Furthermore, it has been confirmed that the formation of $Mg_{20}Ni_8Co_2$ results in a much stronger catalytic action on the hydrogen absorption kinetics of magnesium than Mg_2Ni alone does [26]. The catalytic effect of the $Mg_{20}Ni_{10-x}Co_x$ additive may be ascribed to the inhomogeneity of the alloys containing a $MgNi_2$ phase along with cobalt and nickel clusters. This inhomogeneity is directly associated with the chemisorption of hydrogen and hence facilitates the hydriding reaction. The catalytic effect of Co has been well elaborated by Bobet et al. [27]. Ni is a largely known catalyst, which is utilized for the hydriding reactions. In this work, the catalytic effect of Co substitution on the hydrogen absorption kinetics of the as-spun Mg_2Ni alloy is ascribed to the enhanced glass forming ability caused by Co substitution. Lee et al. [28] have made efforts to improve the hydrogen sorption properties of Mg by mechanical grinding in H_2 (reactive grinding) with Co, finding that the addition of smaller particles of Co (0.5−1.5 μm) exerts a significant impact on the hydrogen sorption properties of Mg. It has been reckoned that Co with smaller particle sizes may act as a grain refiner for the magnesium. In addition, the expansion and contraction of the particles of Mg during the hydriding/dehydriding cycling also make them finer. Therefore, the addition of Co with smaller particle sizes as well as the hydriding/dehydriding cycling will aid the particles of magnesium to exhibit the higher hydrogen sorption rates. Based on the above mentioned discussion, it can be concluded that the substitution of Co for Ni produces a significant catalytic effect on the hydrogen absorption and desorption capacity and kinetics of Mg and Mg-based alloy. However, it must be pointed out that the action mechanism of Co additive is directly associated with the preparation technology of the alloy.

The electrochemical hydrogen storage kinetics of an alloy is symbolized by its high rate discharge ability (HRD). Fig. 15 describes the evolution of the HRD values of the alloys with the discharge current density. It is fully evident that the HRD values are notably enhanced by both melt spinning and Co substitution. In order to visually describe the influences of the melt spinning and Co substitution on the HRD values of the alloys, The HRD values ($\boldsymbol{i}$=100 mA/g) as the functions of the spinning rate and the Co content are also plotted in Fig. 15, respectively. It can be derived from Fig. 15 that the HRD value ($\boldsymbol{i}$=100 mA/g) of the Co_4 alloy is enhanced from 60.3 to 76.0% by increasing the spinning rate from 0 to 30 m/s, and that of the as-spun (20 m/s) alloys is markedly increased from 63.54 to 75.32% by rising Co content from 0 to 4. It has come to light clearly that high rate discharge ability (HRD) basically

depends on the charge transfer at the alloy-electrolyte interface and the hydrogen diffusion process from the interior of the bulk to the surface of alloy particle [29]. The substitution of Co for Ni notably enhances the HRD values of the alloys, to be attributed to an impactful positive action of Co substitution on the hydrogen diffusion in the alloy. Furthermore, Co substitution accelerates the formation of a concentrated metallic Ni layer on the surface of the alloy electrode which is highly beneficial to enhance the electrochemical catalytic property and to improve the reaction rate of hydrogen [29]. The hydrogen diffusion coefficients in the as-cast and spun alloys were measured using the potential step technique. Fig. 16 depicts the semilogarithmic curves of anodic current versus working duration of the as-cast and spun alloys. It can be seen from Fig. 16 (a) that the melt spinning has a positive effect on the hydrogen diffusion in the Co_4 alloy. Fig.16 (b) exhibits that an increase in the Co content gives rise to a growth in the D value. The above-mentioned results clarify that hydrogen diffusion ability is a crucial factor of the hydrogen absorption kinetics of the alloy.

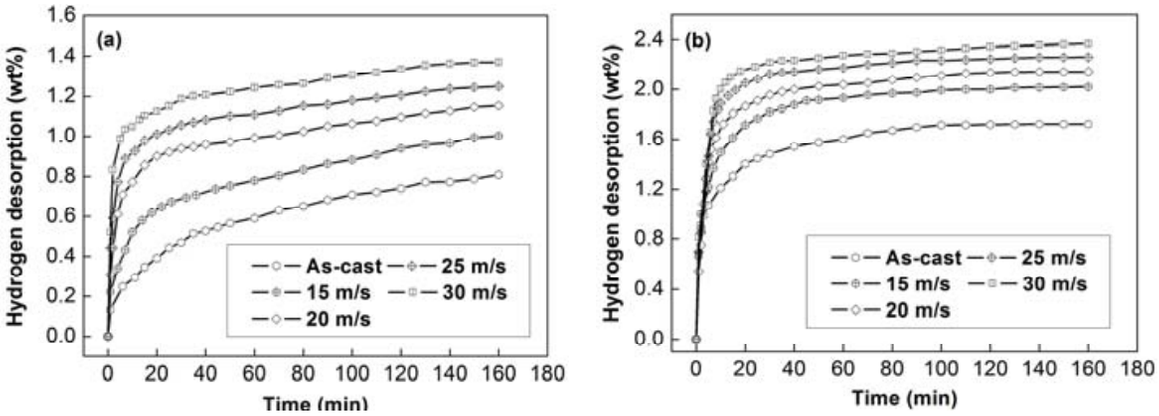

Figure 14. Hydrogen desorption curves of as-cast and spun alloys: (a) Co_1 alloy, (b) Co_4 alloy

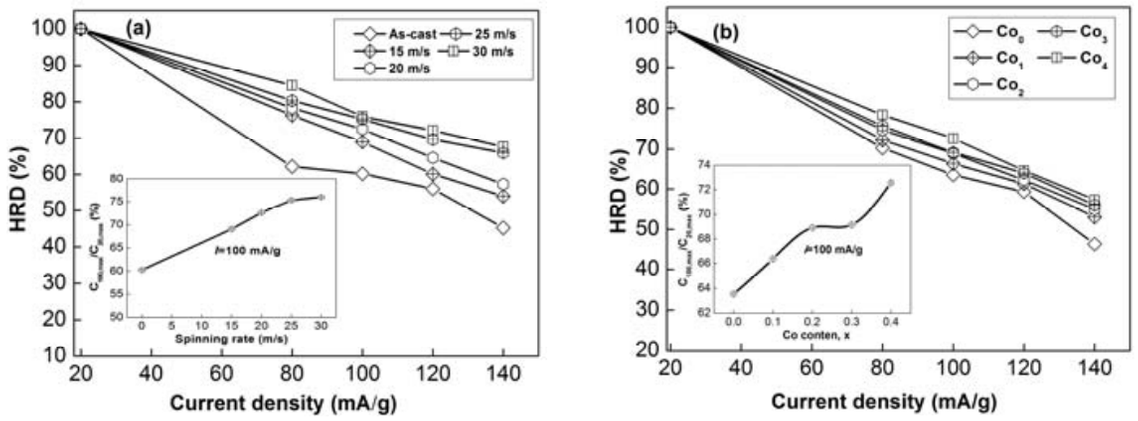

Figure 15. Evolution of the high rate discharge ability (HRD) of the alloys with the discharge current density: (a) Co_4 alloy, (b) As-spun (20 m/s)

Fig. 17 shows the electrochemical impedance spectra (EIS) of the as-spun (15 m/s) alloy electrodes at 50% DOD. It shows that each EIS spectrum contains two semicircles followed by a straight line. According to Kuriyama et al. [30], the smaller semicircle in the high

frequency region is attributed to the contact resistance between the alloy powder and the conductive material, while the larger semicircle in the low frequency region is attributed to the charge-transfer resistance on the alloy surface. The linear response at low frequencies is indicative of hydrogen diffusion in the bulk alloy. Hence, the electrode kinetics of the as-spun alloys are dominated a mixed rate-determining process. It can be seen from Fig. 16 that the radius of the large semicircle in the low frequency visibly decreases with the increasing Co content, implying that the refined grain by Co substitution facilitates charge-transfer resistance of the alloy electrode.

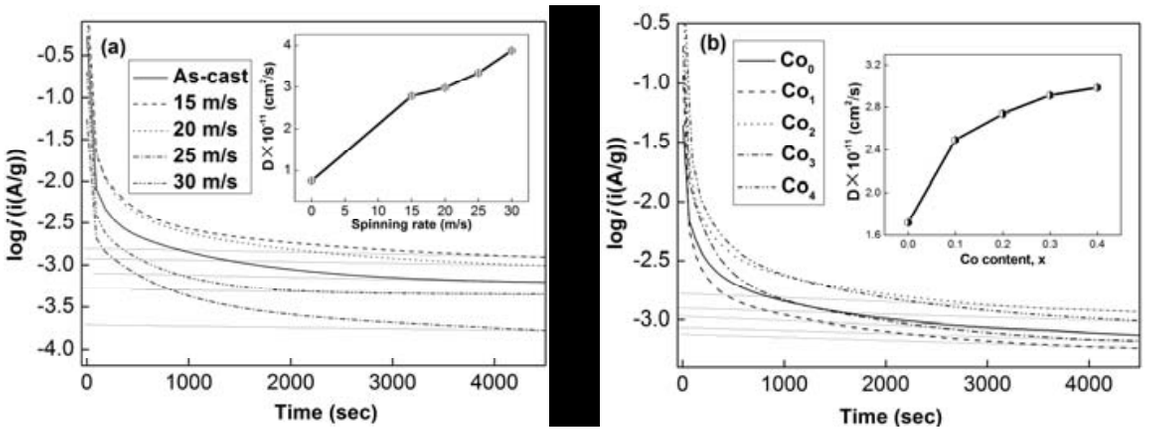

Figure 16. Semilogarithmic curves of anodic current vs. time responses of the alloys: (a) Co_4 alloy, (b) As-spun (20 m/s)

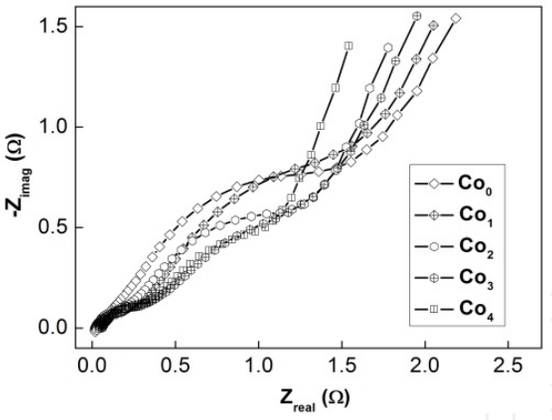

Figure 17. Electrochemical impedance spectra (EIS) of as-spun (15 m/s) alloy electrodes at 50% depth of discharge (DOD)

To determine the kinetics of hydrogen absorption/desorption, Tafel polarization measurements were carried out on the experimental alloy electrodes. Fig. 18 shows the Tafel polarization curves of the as-spun (15 m/s) alloy electrodes at the 50% DOD. It indicates that, in all cases, the anodic current densities increase to a limiting value, then decrease. The existence of a limiting current density, I_L, suggests the forming of an oxidation layer on the surface of the alloy electrode, which resists further penetration of hydrogen atoms [21]. The decrease of the anodic charge current density during cycling implies that charging is

becoming more difficult. Hence, the limiting current density, I_L, may be regarded as a critical passivation current density, which limiting current density, which obtained from the

Tafel polarization curves is also presented in Fig. 18. It can be seen from Fig. 18 that I_L values of the alloys notably increase with rising of the Co content. With an increase in Co content from 0 to 4, the I_L value of the as-spun (15 m/s) alloy increases from 46.7 to 191.7 mA/g, indicating a higher rate of hydrogen diffusion caused by substituting Ni with Co. Based on the factors mentioned above, it can be concluded that the substitution of Co for Ni produces a significant improvement on the hydrogen storage kinetics of Mg_2Ni-type alloy. However, it must be pointed out that the action mechanism of Co substitution is directly associated with the preparation technology of the alloy.

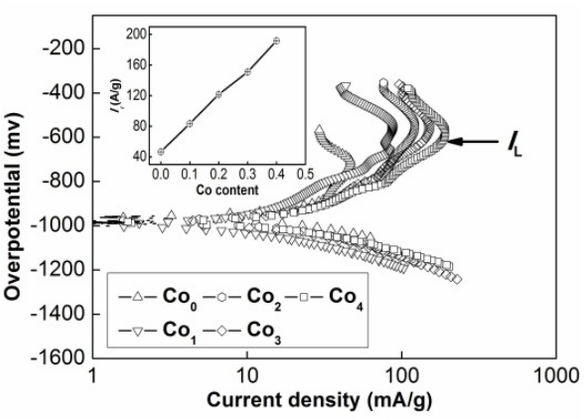

Figure 18. Tafel polarization curves of as-spun (15 m/s) alloy electrodes at 50% DOD and evolution of limiting current density (I_L) with Co content

4.3. The effect of substituting Ni with Cu on microstructure characteristics and gaseous as well as electrochemical hydriding and dehydriding kinetics

4.3.1. Microstructure characteristics

The XRD profiles of the as-cast and spun (25 m/s) alloys are shown in Fig. 19. It is evident that all the as-cast and spun alloys display a single phase structure. Both the substitution of

Cu for Ni and the melt spinning treatment do not change the Mg_2Ni major phase of the alloys. Based on the XRD data, the lattice parameters, cell volume and full width at half maximum (FWHM) values of the main diffraction peaks of the as-cast and spun (25 m/s) alloys were calculated by software of Jade 6.0. The obtained results are listed in Table 2. It is found from Table 2 that the melt spinning renders not only an evident enlargement in the lattice parameters and cell volume, but also a visibly increase in the FWHM values of the main diffraction peaks of the alloys, which is doubtless attributed to the refined average grain size and stored stress in the grains produced by melt spinning. Based on the FWHM values of the broad diffraction peak (203) in Fig. 19, the grain size D_{hkl} (nm) of the as-spun alloy was calculated using Scherrer's equation, which ranging from 2 to 6 nm, consistent with the results reported by Friedlmeier et al. [31].

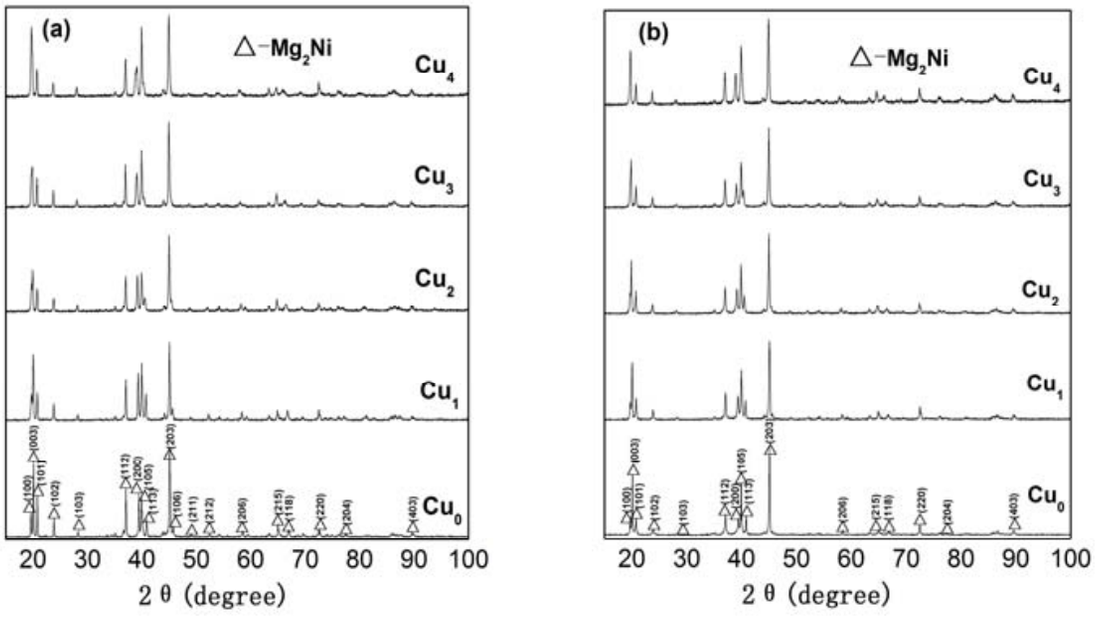

Figure 19. XRD patterns of the as-cast and spun alloys: (a) as-cast, (b) as-spun (25 m/s)

Alloys	FWHM values				Lattice parameters and cell Volume					
	2θ(20.02°)		2θ(45.14°)		a (nm)		c (Å)		V (Å^3)	
	As-cast	25 m/s	As-cast	25 m/s	As-cast	25 m/s	As-cast	25 m/s	As-cast	25 m/s
Cu_0	0.122	0.131	0.169	0.179	5.2097	5.2105	13.244	13.265	311.29	311.88
Cu_1	0.133	0.241	0.178	0.237	5.2102	5.2158	13.252	13.277	311.54	312.79
Cu_2	0.148	0.258	0.183	0.242	5.2136	5.2172	13.283	13.311	312.67	313.76
Cu_3	0.151	0.282	0.192	0.259	5.2154	5.2185	13.297	13.319	313.22	314.11
Cu_4	0.165	0.292	0.204	0.273	5.2171	5.2210	13.302	13.323	313.54	314.50

Table 2. The lattice parameters, cell volume and the FWHM values of the major diffraction peaks of the alloys

The SEM images of the as-cast alloy are presented in Fig. 20, displaying a typical dendrite structure. The substitution of Cu for Ni renders an evident refinement of the grains instead of changing the morphology of the alloys. The result obtained by EDS indicates that the major phase of the as-cast alloys is Mg_2Ni phase (denoted as A). Some small massive matters in the alloys substituted by Cu can clearly be seen in Fig. 20, which are determined by EDS to be Mg_2Cu phase (denoted as B), this apparently contrary to the result of XRD observation. It is most probably associated with the fact that the amount of the Mg_2Cu phase is rare so that the XRD observation can not detect it.

The HRTEM micrographs and electron diffraction patterns of the as-spun (30 m/s) Cu_2 and Cu_4 alloys are illustrated in Fig. 21, exhibiting a nanocrystalline microstructure with an

average crystal size of about 2 nm to 5 nm. It is found from HRTEM observations that the as-spun alloys are strongly disordered and nano-structured, but no amorphous phase is detected, which consistent with the XRD observation. The crystal defects in the as-spun alloy, stacking faults (denoted as A), twin-grain boundary (denoted as B), dislocations (denoted as C) and sub-grain boundary (denoted as D), are clearly viewable in Fig. 22.

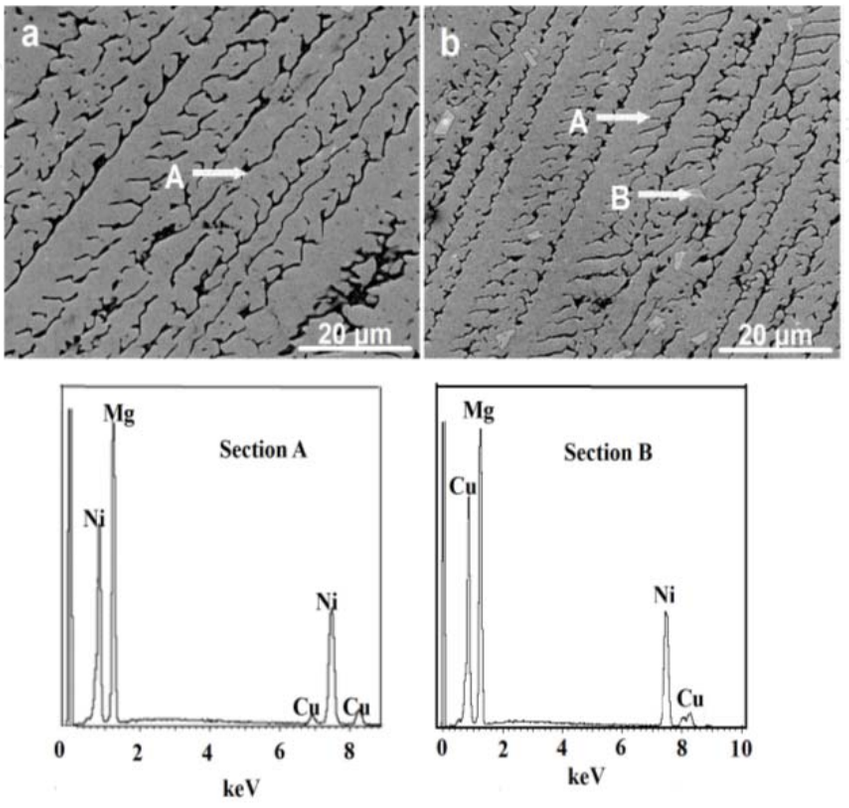

Figure 20. SEM images of the as-cast alloys together with typical EDS spectra of sections A and B in Fig.2b: (a) Cu_0 alloy, (b) Cu_3 alloy

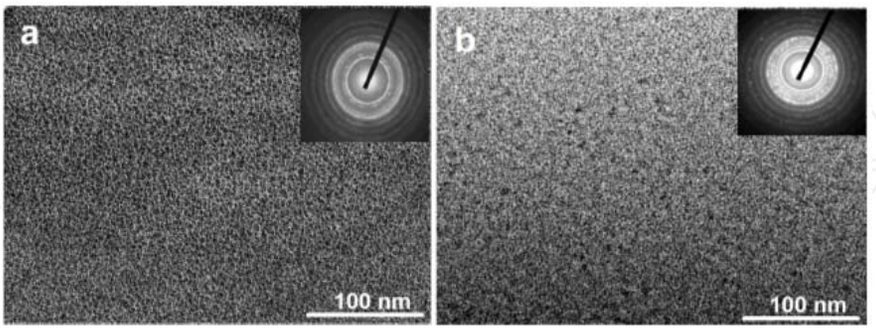

Figure 21. HRTEM images and ED patterns of the as-spun (30 m/s) alloys: (a) Cu_2 alloy, (b) Cu_4 alloy

4.3.2. Gaseous and electrochemical hydriding and dehydriding kinetics

The hydrogen absorption kinetic curves of the as-cast and spun (25 m/s) alloys are plotted in Fig. 23. It is quite evident that the hydrogen absorption capacity of the alloys is visibly enhanced by substituting Ni with Cu. It is noteworthy that, as the amount of Cu substitution

increased to 3, such substitution causes a decline of hydrogen absorption capacity, which primarily attributed to the increase of the $MgCu_2$ phase due to the fact the hydrogen absorption capability of the $MgCu_2$ phase is very low. It is viewed from Fig. 23 (a) that the substitution of Cu for Ni markedly ameliorates the hydrogen absorption kinetics of the as-cast alloys, to be ascribed to the increased cell volume and the refined grain caused by Cu substitution in virtue of the grain boundary possessing the largest hydrogen absorption capability [22].

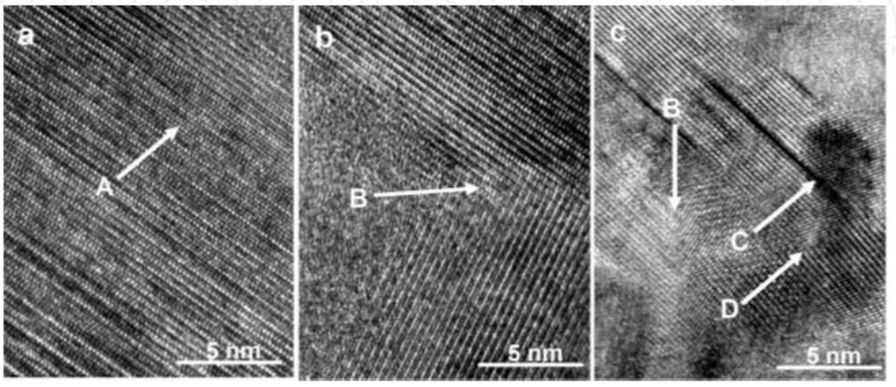

Figure 22. defects in the as-spun (30 m/s) Cu_4 alloy taken by HRTEM: (a) stacking fault, (b) twin-grain boundary, and (c) dislocations and sub-grain boundaries

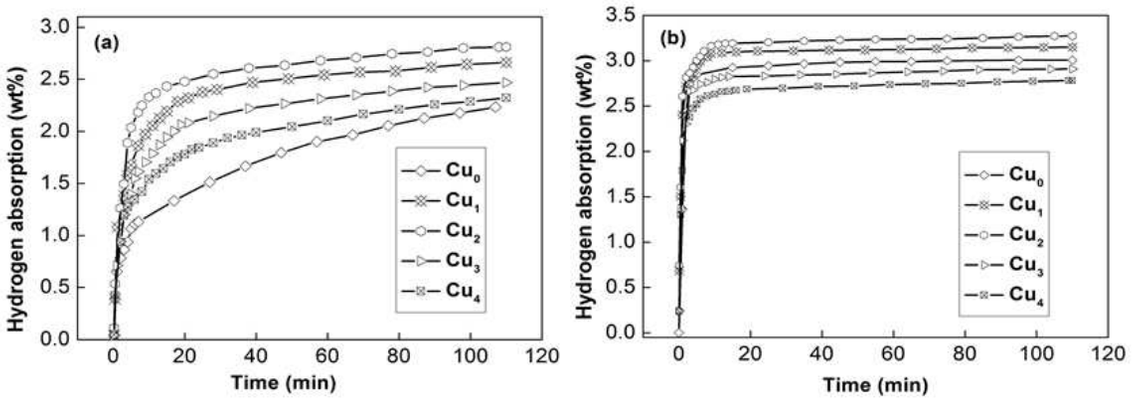

Figure 23. Hydrogen absorption kinetic curves: (a) as-cast, (b) as-spun alloys(25 m/s)

The hydrogen absorption capacity and kinetics of the as-cast and spun Cu_1 and Cu_3 alloys are shown in Fig. 24. It is viewable that the melt spinning evidently improves the hydrogen absorption property of the alloys. The hydrogen absorption capacity in 10 min is increased from 1.99 to 3.12 wt% for Cu_1 alloy, and from 1.74 to 2.88 wt% for the Cu_3 alloy by the increasing spinning rate form 0 (As-cast was defined as spinning rate of 0 m/s) to 30 m/s. It is fully evident that the hydrogen absorption capacity kinetics of all the as-spun nanocrystalline and amorphous Mg_2Ni-type alloys studied are superior to those of conventional polycrystalline materials with the same composition. The improved hydrogenation characteristics are attributed to the enhanced hydrogen diffusivity in the nanocrystalline microstructure as the nanocrystalline leads to an easier access of hydrogen to the nano-sized grains, avoiding the long-range diffusion of hydrogen through an already

formed hydride, which is often the slowest stage of absorption [22]. It is known that the nanocrystalline microstructures can accommodate higher amounts of hydrogen than the polycrystalline ones. The large number of interfaces and grain boundaries available in the nanocrystalline materials provide easy pathways for hydrogen diffusion and promote the absorption of hydrogen.

Fig. 25 describes the influence of substituting Ni with Cu on the hydrogen desorption kinetics of the as-cast and spun alloys. It is observable that both the hydrogen desorption capacity and the kinetics of the alloys increase with the growing amount of Cu substitution. With the increase in Cu content from 0 to 4, the hydrogen desorption capacity in 10 min rises from 0.11 to 0.56 wt% for the as-cast alloy, and from 0.56 to 1.31 wt% for the as-spun (25 m/s) alloy. The enhanced hydrogen desorption kinetics can be ascribed to the fact that the substitution of Cu for Ni in the Mg_2Ni compound decreases the stability of the hydride and makes the desorption reaction easier [12,24]. A similar result was reported by Simićić et al. [32].

The hydrogen desorption kinetic curves of the as-cast and spun alloys are shown in Fig. 26. The figures display that the dehydriding capability of the alloys notably meliorated with the rising of the spinning rate. The hydrogen desorption capacity in 10 min is increased from 0.21 to 0.83 wt% for the Cu_1 alloy, and from 0.44 to 1.29 wt% for the Cu_3 alloy by enhancing of spinning rate from 0 to 30 m/s. It is found that the as-spun nanocrystalline Mg_2Ni alloy exhibits a superior hydrogen desorption kinetics comparing to the crystalline Mg_2Ni, which consistent with the result reported by Spassov et al. [15]. The observed essential differences in the hydriding/dehydriding kinetics of the melt-spun nanocrystalline Mg_2Ni type alloys studied are most probably being associated with the composition of the alloys as well as the differences in their microstructure due to the different spinning rates. It was reported that the high surface to volume ratios, i.e. high specific surface area, and the presence of large numbers of grain boundaries in nanocrystalline alloys enhance the hydriding and dehydriding kinetics [24]. Zaluski et al. [33] and Orimo et al. [34] validated that the hydriding/dehydriding kinetics of the milled nanocrystalline Mg_2Ni alloys at low temperatures (lower than 200 °C) can be improved by reducing the grain size, due to the fact that hydrogen atoms mainly occupied in the disordered interface phase and the grain boundary.

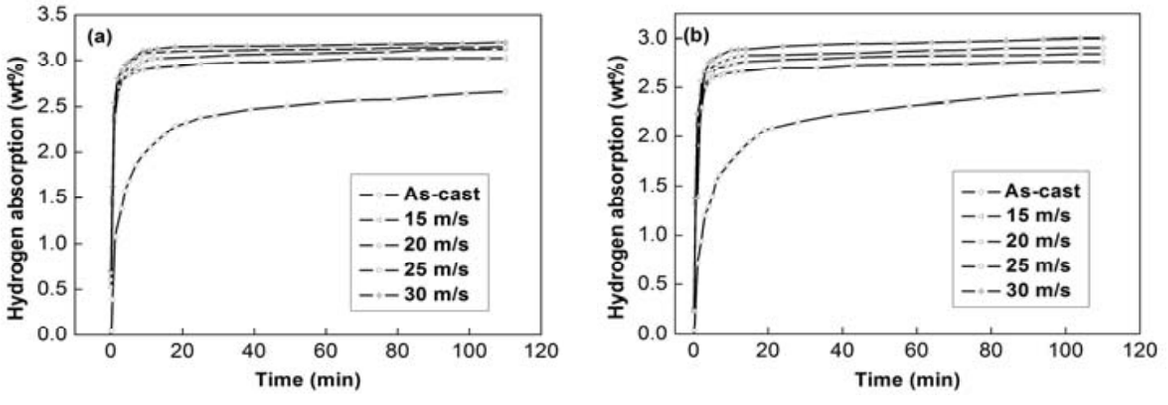

Figure 24. Hydrogen absorption kinetic curves of the as-cast and spun alloys: (a) Cu_1 alloy, (b) Cu_3 alloy

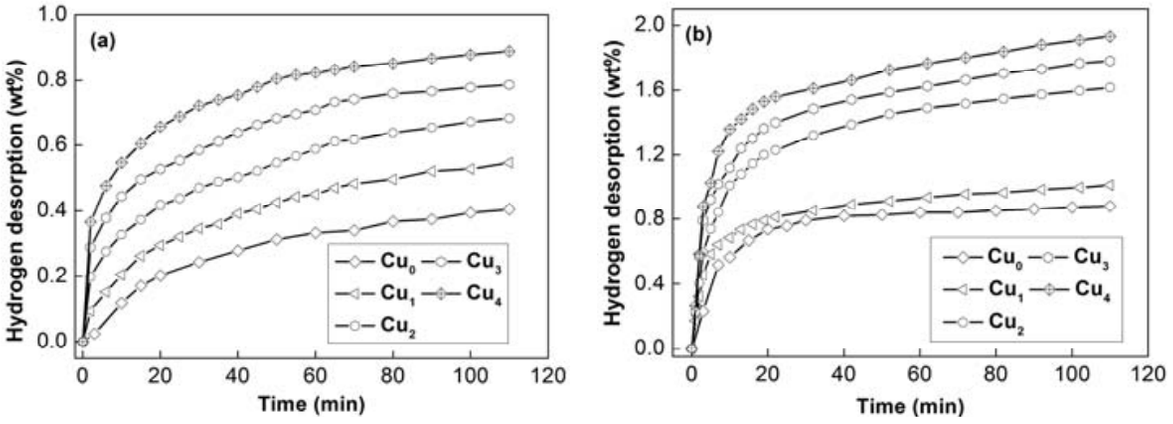

Figure 25. Hydrogen desorption kinetic curves : (a)the as-cast, (b)as-spun alloys (25 m/s)

Fig. 27 describes the evolution of the HRD values of the alloys with the discharge current density. It shows that the HRD values are visibly enhanced by both Cu substitution and melt spinning. In order to visually indicate the influences of the Cu substitution and melt spinning on the HRD values of the alloys, the HRD values (i=100 mA/g) as the functions of the Cu content and the spinning rate are also plotted in Fig. 27, respectively. It can be derived from Fig. 27 that the HRD value (i=100 mA/g) of the as-spun (30 m/s) alloys is markedly increased from 62.4 to 78.9% by rising the Cu content from 0 to 4, and that of the Cu_4 alloy is enhanced from 44.8 to 78.9% by increasing the spinning rate from 0 to 30 m/s.

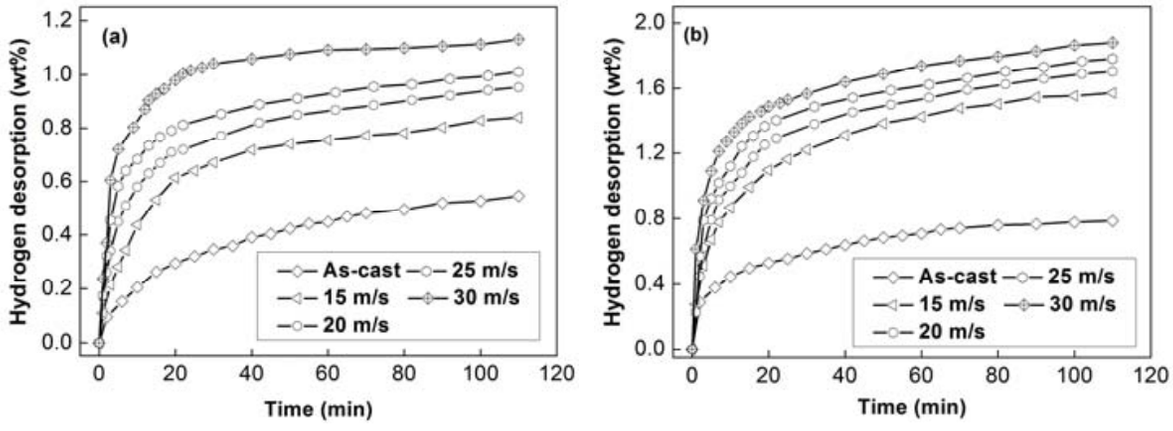

Figure 26. Hydrogen desorption kinetic curves of the as-cast and spun alloys: (a) Cu_1 alloy, (b) Cu_3 alloy

It has come to light clearly that high rate discharge ability (HRD) is basically dominated by the hydrogen diffusion process from the interior of the bulk to the surface of alloy particle and the charge transfer at the alloy-electrolyte interface [35]. The hydrogen diffusion coefficients in the as-cast and spun alloys were measured using the potential step technique. Fig. 28 presents the semilogarithmic curves of anodic current versus working duration of the as-cast and spun alloys. The D values calculated by Eq. (2) are also presented in Fig. 28. It indicates that an increase in the Cu content turns out a growth in the D value. It can be seen

in Fig.28 (b) that the melt spinning has a positive effect on the hydrogen diffusion in the Cu_4 alloy. The above-mentioned results clarify that hydrogen diffusion ability is a crucial factor of the hydrogen absorption kinetics of the alloy.

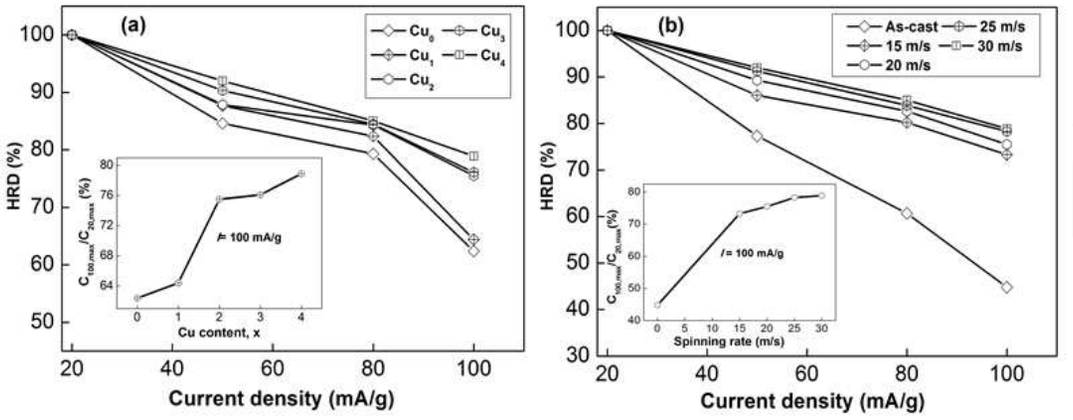

Figure 27. Evolution of the high rate discharge ability (HRD) of the alloys with the discharge current density: (a) As-spun (30 m/s), (b) Cu_4 alloy

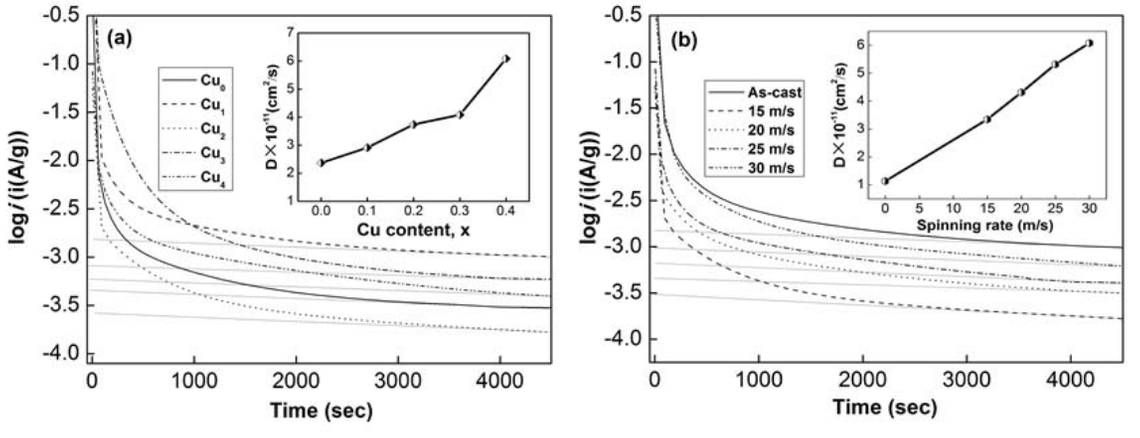

Figure 28. Semilogarithmic curves of anodic current vs. time responses of the as-cast and spun alloys: (a) as-spun (30 m/s), (b) Cu_4 alloy

5. Conclusion

The Mg_2Ni-type $Mg_{20-x}La_xNi_{10}$ (x=0-6) and $Mg_{20}Ni_{10-x}M_x$ (M= Co, Cu; x=0~4) alloys with a nanocrystalline and amorphous structure were successfully fabricated by melt spinning technology. We looked carefully at the SEM, XRD, HRTEM images of the as-cast and spun alloys and did find the formation of amorphous structure in alloys is which attributed to the substitute element and the melt spinning. Our investigation indicated that the substitution of La for Mg and Co for Ni notably enhances the glass forming ability of the Mg_2Ni-type. The amorphized degree of the alloys is associated with the spinning rate. The higher the spinning rate is, the larger the amount of the amorphous phase will be. The quenching rate induced a light influence on the crystallization temperature of the amorphous phase, and it

significantly improved the initial hydrogenation rate and the hydrogen absorption capacity of the alloys.

1. Rapid quenching caused an insignificant change of the phase structure of the La_0 alloy, but it led to a great variety of the phase structure of the La_2 alloy. There was no amorphous phase in the as-quenched La_0 alloy, whereas the as-quenched La_2 alloy presented a feature of the nanocrystalline embedded in the amorphous matrix, which ascribed to the fact that the substitution of La for Mg significantly enhanced the glass forming ability of the $Mg_{20-x}La_xNi_{10}$ (x = 0, 2) hydrogen storage alloys. Rapid quenching markedly increased the hydrogen absorption and desorption capacities and kinetics of the $Mg_{20-x}La_xNi_{10}$ (x = 0, 2) alloys, which mainly ascribed to the nanocrystalline and amorphous microstructures formed by rapid quenching.
2. The substitution of Co for Ni does not alter the major phase of Mg_2Ni but results in the formation of the secondary phase $MgCo_2$. No amorphous phase is detected in the as-spun Co-free alloy, but a certain amount of amorphous phase is clearly found in the as-spun Co-containing alloys. The substitution of Co for Ni exerts a slight influence on the hydriding kinetics of the as-spun alloy. However, it dramatically enhances the dehydriding kinetics of the as-cast and spun alloys.
3. The substitution of Cu for Ni leads to the formation of the secondary phase Mg_2Cu in the as-cast alloys instead of changing of the Mg_2Ni-type major phase in the alloy. Additionally, Cu substitution visibly refines the grains of the as-cast alloy, whereas it causes an imperceptible impact on the glass forming ability of the alloy. With the increase in the amount of Cu substitution, the hydrogen absorption capacity of the as-cast Mg_2Ni-type alloys first increases and then decreases. But it markedly improves the hydrogen desorption capability of the as-cast and spun alloys. Melt spinning evidently promotes the hydriding and dehydriding performances of the Mg_2Ni-type alloys. Hydriding/dehydriding capacities and rates of the alloys markedly rise with the increasing of the spinning rate.

Author details

Yanghuan Zhang, Hongwei Shang, Chen Zhao and Dongliang Zhao
Department of Functional Material Research, Central Iron and Steel Research Institute, China

Yanghuan Zhang, Hongwei Shang and Chen Zhao
Elected State Key Laboratory, Inner Mongolia University of Science and Technology, China

6. References

[1] Das, D., Veziroglu, TN. Hydrogen production by biological processes: a survey of literature. International Journal of Hydrogen Energy 2001; 26 (1) 13-28.

[2] Frackowiak, E., Be´guin, F. Electrochemical storage of energy in carbon nanotubes and nanostructured carbons. Carbon 2002; 40 (10) 1775-1787.

[3] Reilly, JJ., Adzic, GD., Johnson, JR., Vogt, T., Mukerjee, S., Mcbreen, J. The correlation between composition and electrochemical properties of metal hydride electrodes. Journal of Alloys and Compounds 1999; 293–295 569-582.

[4] Jain, IP., Lal, C., Jain, A. Hydrogen storage in Mg: A most promising material. International Journal of Hydrogen Energy 2010; 35 (10) 5133-5144.

[5] Jain, IP. Hydrogen the fuel for 21st century. International Journal of Hydrogen Energy 2009; 34 (17) 7368-7378.

[6] Kwon, SN., Baek, SH., Mummb, DR., Hong, SH., Song, MY. Enhancement of the hydrogen storage characteristics of Mg by reactive mechanical grinding with Ni, Fe and Ti. International Journal of Hydrogen Energy 2008; 33 (17) 4586-4592.

[7] Palade, P., Sartori, S., Maddalena, A., Principi, G., Lo, Russo S, Lazarescu M, Schinteie G, Kuncser V, Filoti G. Hydrogen storage in Mg–Ni–Fe compounds prepared by melt spinning and ball milling. Journal of Alloys and Compounds 2006; 415 (1-2) 170-176.

[8] Spassov, T., Köster, U. Hydrogenation of amorphous and nanocrystalline Mg-based alloys. Journal of Alloys and Compounds. 1999; 287 (1-2) 243–250.

[9] Orimo, S., Fujii, H. Hydriding properties of the Mg_2Ni-H system synthesized by reactive mechanical grinding. Journal of Alloys and Compounds 1996; 232 (1-2) L16–L19.

[10] Inoue, A., Masumoto, T. Mg-based amorphous alloys. Materials Science and Engineering A. 1993; 173 (1-2) 1–8.

[11] Kim, S.G., Inoue, A., Masumoto, T. High Mechanical Strengths of Mg–Ni–Y and Mg–Cu–Y Amorphous Alloys with Significant Supercooled Liquid Region. Materials Transactions, JIM 1990; 31 (11) 929–934.

[12] Woo, JH., Lee, KS. Electrode characteristics of nanostructured Mg_2Ni-type alloys prepared by mechanical alloying. Journal of the Electrochemical Society 1999; 146 (3) 819-823.

[13] Liang, G. Synthesis and hydrogen storage properties of Mg-based alloys. Journal of Alloys and Compounds 2004; 370 (1-2) 123–128.

[14] Song, MY., Kwon, SN., Bae, JS., Hong, SH. Hydrogen-storage properties of Mg–23.5Ni–(0 and 5)Cu prepared by melt spinning and crystallization heat treatment. International Journal of Hydrogen Energy 2008; 33 (6) 711-1718.

[15] Spassov, T., Köster, U. Thermal stability and hydriding properties of nanocrystalline melt-spun $Mg_{63}Ni_{30}Y_7$ alloy. Journal of Alloys and Compounds 1998; 279 (2) 279–286.

[16] Huang, LJ., Liang, GY., Sun, ZB., Wu, DC. Electrode properties of melt-spun Mg–Ni–Nd amorphous alloys. Journal of Power Sources 2006; 160 (1) 684-687.

[17] Yamaura, SI., Kim, HY., Kimura, H., Inoue, A., Arata, Y. Thermal stabilities and discharge capacities of melt-spun Mg–Ni-based amorphous alloys. Journal of Alloys and Compounds. 2002; 339 (1-2) 230-235.

[18] Chen, H.S. Thermodynamic considerations on the formation and stability of metallic glasses. Acta Metallurgica 1974; 22(12) 1505-1511.

[19] Spassov, T., Solsona, P., Suri˜nach, S., Baró, MD. Optimisation of the ball-milling and heat treatment parameters for synthesis of amorphous and nanocrystalline Mg_2Ni-based alloys. Journal of Alloys and Compounds 2003; 349 (1-2) 242–254.

[20] Zheng, G., Popov, BN., White, RE. Electrochemical Determination of the Diffusion Coefficient of Hydrogen Through an $LaNi_{4.25}Al_{0.75}$ Electrode in Alkaline Aqueous Solution. Journal of the Electrochemical Society 1995; 142 (8) 2695-2698.

[21] Niu, H., Derek, ON. Enhanced electrochemical properties of ball-milled Mg_2Ni electrodes. International Journal of Hydrogen Energy 2002; 27 (1) 69-77.

[22] Orimo, S., Fujii, H. Materials science of Mg-Ni-based new hydrides. Applied Physics A, 2001; 72 (2) 167−186.

[23] Goo, NH., Jeong, WT., Lee, KS. The hydrogen storage properties of new Mg_2Ni alloy. Journal of Power Sources 2000; 87 (1-2) 118-124.

[24] Takahashi, Y., Yukawa, H., Morinaga, M. Alloying effects on the electronic structure of Mg_2Ni intermetallic hydride. Journal of Alloys and Compounds 1996; 242 (1-2) 98−107.

[25] Khrussanova, M., Grigorova, E., Bobet, J.-L., Khristov, M., Peshev, P. Hydrogen sorption properties of the nanocomposites Mg-$Mg_2Ni_{1-x}Co_x$ obtained by mechanical alloying. Journal of Alloys and Compounds 2004; 365 (1-2) 308−313.

[26] Khrussanova, M., Mandzhukova, T., Grigorova, E., Khristov, M., Peshev, P. Hydriding properties of the nanocomposite 85wt.%Mg-15wt.% $Mg_2Ni_{0.8}Co_{0.2}$ obtained by ball milling. Journal of Materials Science, 2007; 42 (10) 3338−3342.

[27] Bobet JL., Chevalier B., Darriet B. Effect of reactive mechanical grinding on chemical and hydrogen sorption properties of the Mg+10wt.%Co mixture. Journal of Alloys and Compounds 2002; 330-320 738-742.

[28] Lee, DS., Kwon, IH., Bobet, JL., Song, MY. Effects on the H_2-sorption properties of Mg of Co (with various sizes) and CoO addition by reactive grinding. Journal of Alloys and Compounds 2004; 366 (1-2) 279−288.

[29] Gasiorowski A., Iwasieczko W., Skoryna D., Drulis H., Jurczyk M. Hydriding properties of nanocrystalline Mg2−xMxNi alloys synthesized by mechanical alloying (M=Mn, Al). Journal of Alloys and Compounds 2004; 364 (1-2) 283−288.

[30] Kuriyama, N., Sakai T., Miyamura H., Uehara I., Ishikawa H., Iwasaki T. Electrochemical impedance and deterioration behavior of metal. Journal of Alloys and Compounds 1993; 202 (1-2) 183−197.

[31] Friedlmeier, G., Arakawa, M., Hiraia, T., Akiba, E. Preparation and structural, thermal and hydriding characteristics of melt-spun Mg-Ni alloys. Journal of Alloys and Compounds 1999; 292 (1) 107−117.

[32] Simićić, MV., Zdujić, M., Dimitrijević, R. Hydrogen absorption and electrochemical properties of Mg_2Ni-type alloys synthesized by mechanical alloying. Journal of Power Sources 2006; 158 (1) 730-734.

[33] Zaluski, L., Zaluska, A., Strön-Olsen, JO. Nanocrystalline metal hydrides. Journal of Alloys and Compounds 1997; 253-254 70-79.

[34] Orimo, S., Fujii, H., Ikeda, K. Notable hydriding properties of a nanostructured composite material of the Mg_2Ni-H system synthesized by reactive mechanical grinding. Acta Materialia 1997; 45 (1) 331-341.

[35] Wu, Y., Han, W., Zhou, SX., Lototsky, MV., Solberg, JK., Yartys, VA. Microstructure and hydrogenation behavior of ball-milled and melt-spun Mg-10Ni-2Mm alloys. Journal of Alloys and Compounds 2008; 466 (1-2) 176–181.

IntechOpen

IntechOpen